JPn Neuroscience

The Journal of Physiology

J Physiol 591.13 (2013) pp 3253–3269

Harmonin enhances voltage-dependent facilitation of $Ca_v1.3$ channels and synchronous exocytosis in mouse inner hair cells

Frederick D. Gregory[1], Tina Pangršič[2], Irina E. Calin-Jageman[3], Tobias Moser[2] and Amy Lee[1]

[1] *Departments of Molecular Physiology and Biophysics, Otolaryngology-Head and Neck Surgery, and Neurology, University of Iowa, Iowa City, IA, USA*
[2] *InnerEarLab, Department of Otolaryngology and Collaborative Research Center 889, University Medical Center Göttingen, Göttingen, Germany*
[3] *Department of Biological Sciences, Dominican University, River Forest, IL, USA*

Key points

- $Ca_v1.3$ Ca^{2+} channels mediate sound transmission by triggering presynaptic exocytosis of glutamate from cochlear inner hair cells (IHCs).
- Harmonin is a PDZ-domain-containing protein in IHCs that is altered in Usher syndrome, a form of deaf–blindness in humans.
- We show that harmonin enhances $Ca_v1.3$ voltage-dependent facilitation (VDF) in transfected HEK293T cells in a manner that depends on the identity of the auxiliary Ca^{2+} channel β subunit.
- $Ca_v1.3$ VDF is impaired, and synchronous exocytosis and the Ca^{2+} efficiency of exocytosis are reduced, in IHCs from deaf-circler mice expressing a mutant form of harmonin (*dfcr*) that cannot interact with $Ca_v1.3$.
- We conclude that harmonin regulates presynaptic function in mouse IHCs, which adds to our understanding of the factors that may influence hearing impairment in Usher syndrome.

Abstract $Ca_v1.3$ channels mediate Ca^{2+} influx that triggers exocytosis of glutamate at cochlear inner hair cell (IHC) synapses. Harmonin is a PDZ-domain-containing protein that interacts with the C-terminus of the $Ca_v1.3$ α_1 subunit ($\alpha_1$1.3) and controls cell surface $Ca_v1.3$ levels by promoting ubiquitin-dependent proteosomal degradation. However, PDZ-domain-containing proteins have diverse functions and regulate other $Ca_v1.3$ properties, which could collectively influence presynaptic transmitter release. Here, we report that harmonin binding to the $\alpha_1$1.3 distal C-terminus (dCT) enhances voltage-dependent facilitation (VDF) of $Ca_v1.3$ currents both in transfected HEK293T cells and in mouse inner hair cells. In HEK293T cells, this effect of harmonin was greater for $Ca_v1.3$ channels containing the auxiliary Ca_v β_1 than with the β_2 auxiliary subunit. $Ca_v1.3$ channels lacking the $\alpha_1$1.3 dCT were insensitive to harmonin modulation. Moreover, the 'deaf-circler' *dfcr* mutant form of harmonin, which does not interact with the $\alpha_1$1.3 dCT, did not promote VDF. In mature IHCs from mice expressing the *dfcr* harmonin mutant, $Ca_v1.3$ VDF was less than in control IHCs. This difference was not observed between control and *dfcr* IHCs prior to hearing onset. Membrane capacitance recordings from *dfcr* IHCs revealed a role for harmonin in synchronous exocytosis and in increasing the efficiency of Ca^{2+} influx for triggering exocytosis. Collectively, our results indicate a multifaceted presynaptic role of harmonin in IHCs in regulating $Ca_v1.3$ Ca^{2+} channels and exocytosis.

F. D. Gregory and T. Pangršič contributed equally to this work.

DOI: 10.1113/jphysiol.2013.254367

(Resubmitted 5 March 2013; accepted 16 April 2013; first published online 22 April 2013)
Corresponding authors A. Lee: Department of Molecular Physiology and Biophysics, University of Iowa, 5-610 Bowen Science Building, 51 Newton Rd, Iowa City, IA 52242, USA. Email: amy-lee@uiowa.edu; T. Moser: InnerEarLab, Department of Otolaryngology and Collaborative Research Center 889, University Medical Center Göttingen, Robert-Koch-Str. 40, D-37075 Göttingen, Germany. Email: tmoser@gwdg.de

Abbreviations CDI, Ca^{2+}-dependent inactivation; dCT, distal C-terminus; IHC, inner hair cell; p, postnatal day; RRP, readily releasable pool; VDF, voltage-dependent facilitation; VDI, voltage-dependent inactivation.

Introduction

Voltage-gated $Ca_v1.3$ Ca^{2+} channels are highly expressed in cochlear inner hair cells (IHCs), where their activity is tightly coupled to the exocytic release from specialized 'ribbon' synapses (Platzer *et al.* 2000; Brandt *et al.* 2003). Mice lacking $Ca_v1.3$ are deaf (Platzer *et al.* 2000; Dou *et al.* 2004) as are humans with loss-of-function mutations in the *CACNA1D* gene encoding the pore-forming $Ca_v1.3$ α_1 subunit ($\alpha_1$1.3) (Baig *et al.* 2011). $Ca_v1.3$ channels are subject to diverse forms of regulation, which can strongly impact neuronal and cardiac signalling (Mangoni *et al.* 2003; Olson *et al.* 2005; Hetzenauer *et al.* 2006; Zhang *et al.* 2006; Chan *et al.* 2007; Navedo *et al.* 2007). Therefore, characterization of the factors that modulate $Ca_v1.3$ channels in IHCs is essential for understanding the dynamics of presynaptic Ca^{2+} signals and sound transmission by IHCs.

Like other Ca_v1 channels, $Ca_v1.3$ can interact directly with various proteins (Calin-Jageman & Lee, 2008). The distal C-terminus (dCT) of the $Ca_v1.3$ $\alpha_1$1.3 contains a consensus site for binding to PDZ (PSD-95 (postsynaptic density-95)/Discs large/ZO-1 (zona occludens-1)) domains (Songyang *et al.* 1997). Interactions with PDZ-domain-containing proteins affect the localization and function of $Ca_v1.3$ in neurons (Olson *et al.* 2005; Zhang *et al.* 2005, 2006). One such protein, erbin, binds to the $\alpha_1$1.3 dCT and potentiates $Ca_v1.3$ currents in response to depolarizing stimuli through a process known as voltage-dependent facilitation (VDF; Calin-Jageman *et al.* 2007). Densin-180 also interacts with the $\alpha_1$1.3 dCT but does not enhance $Ca_v1.3$ VDF. Rather, densin-180 tethers calmodulin-dependent protein kinase II to the $Ca_v1.3$ channel complex, which mediates Ca^{2+}-dependent facilitation of $Ca_v1.3$ currents in response to high-frequency repetitive stimuli (Jenkins *et al.* 2010).

Like erbin and densin-180, harmonin is a PDZ-domain-containing protein expressed in the brain, but is additionally localized in IHCs (Verpy *et al.* 2000; Reiners *et al.* 2005). The gene encoding harmonin corresponds to the USH1C locus for Usher Type 1 syndrome (Verpy *et al.* 2000), an autosomal recessive sensory disorder characterized by deafness, vestibular dysfunction, and late-onset retinitis pigmentosa (Kimberling & Moller, 1995). Harmonin is concentrated in the apical hair bundles of cochlear and vestibular hair cells (Adato *et al.* 2005), where it interacts with multiple proteins and regulates mechanotransduction channels that convert mechanical stimuli into changes in hair cell membrane potential (Grillet *et al.* 2009; Michalski *et al.* 2009). In mature IHCs, harmonin is also localized to a subset of ribbon-type active zones. Harmonin binds to the $\alpha_1$1.3 dCT, which enhances proteosomal degradation of $Ca_v1.3$ and controls $Ca_v1.3$ channel density at mouse IHC synapses (Gregory *et al.* 2011). It is not known whether, like erbin and densin-180, harmonin has other modulatory actions on $Ca_v1.3$ that could impact presynaptic function in IHCs. In addition, given the strong localization of harmonin at IHC synapses, harmonin may also play a role in glutamate exocytosis, which has also not been investigated.

To address these open questions, we tested if harmonin influenced additional properties of $Ca_v1.3$, and probed the impact of harmonin on exocytosis in IHCs. We found that like erbin, harmonin enhances $Ca_v1.3$ VDF, which depends on the interaction of harmonin with the $\alpha_1$1.3 dCT and the identity of the $Ca_v\beta$ subunit. Moreover, we established that harmonin regulates $Ca_v1.3$ VDF and exocytosis in mouse IHCs. Our results highlight new roles for harmonin as a regulator of presynaptic function in IHCs.

Methods

Ethical approval

All procedures involving mice were approved by the Institutional Animal Care and Use Committee at the University of Iowa in accordance with National Institutes of Health guidelines and animal welfare guidelines at the University of Göttingen and the State of Lower Saxony. After mice were killed by decapitation (for mice less than 10 days old) or isoflurane overdose and/or decapitation (for mice greater than 10 days old), the skull was opened, and the cochlea was removed and opened at the apex so that the apical coil could be harvested for electrophysiological experiments.

Constructs and molecular biology

The following Ca_v subunit cDNAs were used: $\alpha_1 1.3$ containing exon 42 (GenBank no. AF370009 and AF370010 for additional sequence encoded by exon 42), β_{1b} (GenBank no. NM017346), $\alpha_1 1.2$ (GenBank no. M67515), β_{2A} (GenBank no. NM053851), and $\alpha_2\delta$-1 (GenBank no. M21948). Expression constructs for FLAG-tagged $\alpha_1 1.3$, $\alpha_1 1.3_{L-A}$, $\alpha_1 1.3_{exon42A}$, and green fluorescent protein (GFP)- and myc-tagged harmonin, *dfcr* mutant were previously described (Calin-Jageman *et al.* 2007; Gregory *et al.* 2011).

Cell culture and transfection

Human embryonic kidney cells transformed with SV40 T-antigen (HEK293T) were maintained in Dulbecco's modified Eagle's medium with 10% fetal bovine serum (Life Technologies, Grand Island, NY, USA) at 37°C in a humidified atmosphere under 5% CO_2. Cells were grown to ∼60–90% confluence in 100 mm plates and transfected using GenePorter Reagent (Gene Therapy Systems, San Diego, CA, USA). For immunoprecipitation experiments, HEK293T cells were transfected with cDNAs encoding $Ca_v1.3$ (FLAG-$\alpha_1 1.3$, FLAG-$\alpha_1 1.3_{exon42A,}$ or FLAG-$\alpha_1 1.3_{L\text{-}A}$ (6 μg), β_{1b} and $\alpha_2\delta$ (2 μg each)) and myc-harmonin (4 μg). For electrophysiological experiments, cells were plated on 35 mm culture dishes and transiently transfected using Fugene transfection reagent (Promega, Fitchburg, WI, USA). A total of ∼3 μg total DNA was transfected: $\alpha_1 1.3$, 1.5 μg; β, 0.8 μg; $\alpha_2\delta$, 0.8 μg; ±GFP-tagged harmonin or *dfcr* mutant, 0.5 μg; or GFP expression plasmid, 0.01 μg.

Coimmunoprecipitation

HEK293T cells were harvested and lysed 48 h after transfection. Lysates were incubated with ANTI-FLAG M2-Agarose Affinity Gel (all reagents from FLAG Immunoprecipitation Kit, Sigma-Aldrich, St Louis, MO, USA) for 2.5 h, rotating at 4°C. After three washes with wash buffer (provided in the FLAG Immunoprecipitation Kit), proteins were eluted with SDS-containing sample buffer and subjected to SDS-PAGE. Coimmunoprecipitated proteins were detected by Western blotting with antibodies against $\alpha_1 1.3$ (Ab144; Gregory *et al.* 2011) or myc epitopes (Sigma-Aldrich). Following incubation with appropriate secondary antibodies, WesternC reagent (Bio-rad, Hercules, CA, USA) was utilized for development and the Geldoc Imager for image collection (Bio-rad). Quantification was performed densitometrically with Quantity One software (Bio-rad). To obtain the fraction of harmonin that coimmunoprecipited with $\alpha_1 1.3$, Western blot signals corresponding to bands for harmonin were divided by those representing the FLAG-immunoprecipitated $\alpha_1 1.3$. For each experiment, these values for harmonin coimmunoprecipitated with $\alpha_1 1.3_{ex42A}$ or $\alpha_1 1.3_{L\text{-}A}$ were normalized to that for $\alpha_1 1.3$ to determine the percentage change in harmonin that coimmunoprecipitated with $\alpha_1 1.3_{ex42A}$ or $\alpha_1 1.3_{L\text{-}A}$ relative to that for $\alpha_1 1.3$. Data from three independent experiments were averaged (mean ± SEM).

Electrophysiological recordings

Ba^{2+} currents (I_{Ba}) were recorded 48–72 h after transfection at room temperature using the whole-cell patch clamp electrophysiology technique from transiently transfected HEK293T cells. The internal solution contained (in mM): 140 NMDG, 5 EGTA, 10 Hepes, 2 $MgCl_2$, 2 Mg-ATP, pH 7.3 (with methanesulfonate) and adjusted to ∼290 mosmol l^{-1} with glucose. The external solution contained (in mM): 150 Tris, 2 $MgCl_2$, 10 $BaCl_2$, pH 7.35 (with methanesulfonate) and adjusted to ∼310 mosmol l^{-1} with glucose. Pipettes of 3–5 MΩ resistance were used. Voltage clamp recordings were performed with an EPC-9 or EPC-10 amplifier under control of PULSE or Patchmaster software (HEKA Elektronik, Lambrecht, Germany). Currents were filtered at 2 kHz and sampled at 10–20 kHz. A *P*/4 protocol was used to subtract leak currents.

For whole-cell patch clamp recordings of mouse IHCs, cochlear tissue was dissected from mice (postnatal days (p) 6–8 or p16–18) in Minimum Essential Medium (MEM)/Glutamax-1 (Invitrogen, Gaithersburg, MD, USA) supplemented with 10 mM Hepes at room temperature and kept up to 18 h at 37°C prior to recording. IHCs in the apical cochlear turn were visualized on an upright microscope (BX51WI, Olympus) with a ×40 water-immersion objective with DIC optics. The basolateral membrane of IHCs was patch-clamped with electrodes pulled from thick-walled borosilicate glass capillaries (1B150F, Warner Instruments, Camden, CT, USA). The internal solution contained (in mM): 120 caesium gluconate, 80 CsCl, 0.1 $CaCl_2$, 4 MgATP, 5 Hepes and 5 EGTA; pH was adjusted to 7.35 with CsOH; osmolarity ∼305 mosmol l^{-1}. External solution contained (in mM): 105 NaCl, 5.8 KCl, 10 CsCl, 55 TEA-Cl, 10 $BaCl_2$, 1 MgCl, 10 glucose and 10 Hepes supplemented with MEM Vitamins and Amino Acids (Invitrogen, Gaithersburg, MD, USA) at 1X; pH was adjusted to 7.4 with TEA-OH; osmolarity ∼320 mosmol l^{-1}. On the day of recording, 4-aminopyridine (4 mM), apamin (0.3 mM) and TTX (0.5 mM, for p6–8 IHCs) were added to the external solution. Electrode resistances were 3.5–6.2 MΩ in the external solution. Data were acquired with HEKA EPC-9 or EPC-10 amplifiers controlled by Patchmaster software (HEKA Elektronik, Lambrecht, Germany). Leak

subtraction was done online with a *P*/6 protocol. Series resistance was compensated with the patch clamp circuitry (50–70%); average uncompensated series resistance was 12.9 ± 0.6 ($n = 89$ IHCs). Currents were low-pass filtered at 5 kHz and sampled at 20 kHz except for VDF measurements, where currents were filtered at 2.9 kHz and sampled at 10 kHz. Voltages were not corrected for the liquid junction potential of −7 mV in the external recording solution.

Electrophysiological data were analysed with custom routines in IgorPro software (Wavemetrics, Portland, OR, USA). Average data are expressed as mean ± SEM. Statistical comparisons were done using SigmaPlot software (Systat, Chicago, IL, USA).

Confocal Ca^{2+} imaging

Confocal Ca^{2+} imaging was performed in IHCs from *dfcr* mice and their wild-type littermates as described previously (Frank *et al.* 2009; Gregory *et al.* 2011). In brief, synaptic Ca^{2+} microdomains were identified as hotspots of Fluo-5N fluorescence (low affinity Ca^{2+} indicator) in *XY* scans using long (200–254 ms) step depolarizations. We then positioned the laser at the peak pixel of each Ca^{2+} microdomain as identified in the *XY* scan (spot detection) and invoked Ca^{2+} influx by 20 ms step depolarizations to −32 mV. We then applied a 50 ms depolarization to +63 mV preceding the second 20 ms depolarization to −32 mV in order to facilitate the Ca^{2+} influx. The internal solution contained (in mM): 115 caesium glutamate, 13 TEA-Cl, 1 $MgCl_2$, 1 $CaCl_2$, 10 EGTA, 2 ATP-Mg, 0.3 GTP-Na, 20 Hepes (pH adjusted with CsOH to 7.2, osmolarity ∼295 mosmol l^{-1}) and 0.4 Fluo-5N (penta-potassium salt; Invitrogen). The external solution contained (in mM): 102 NaCl, 35 TEA-Cl, 2.8 KCl, 5 $CaCl_2$, 1 $MgCl_2$, 10 Hepes, 1 CsCl, 11.1 D-glucose (pH adjusted with NaOH to 7.2, osmolarity ∼300 mosmol l^{-1}). Data are presented as mean ± SEM, unless otherwise stated.

Capacitance recordings

For capacitance recordings, IHCs from *dfcr* mice and their wild-type littermates (p13–19) were subjected to perforated and ruptured patch-clamp recording as described previously (Moser & Beutner, 2000). The internal solution for perforated-patch experiments contained (in mM): 130 caesium gluconate, 10 TEA-Cl, 10 4-aminopyridine, 1 $MgCl_2$, 10 Hepes (pH adjusted with HCl to 7.17, osmolarity ∼290 mosmol l^{-1}) and 300 μg ml^{-1} amphotericin B. The internal solution for EGTA experiments contained (in mM): 115 caesium glutamate, 13 TEA-Cl, 1 $MgCl_2$, 4 EGTA, 2 $CaCl_2$, 20 Hepes, 2 Mg-ATP, 0.3 Na-GTP (pH adjusted with CsOH to 7.2, osmolarity ∼290 mosmol l^{-1}). The external solution contained (in mM): 100–104 NaCl, 35 TEA-Cl, 2.8 KCl, 10 $CaCl_2$, 1 $MgCl_2$, 10 Hepes, 1 caesium gluconate or CsCl, 5 4-aminopyridine, 11.1 D-glucose (pH adjusted with NaOH to 7.2, osmolarity ∼300 mosmol l^{-1}). For most perforated-patch experiments the external solution also contained apamin (0.1 mM). An EPC-9 amplifier controlled by Pulse software (HEKA Elektronik) was used for measurements. All voltages were corrected for liquid junction potentials. Currents were sampled at 20 kHz and low-pass filtered at 2 kHz. Cells that displayed a holding current exceeding −50 pA were discarded from analysis. Ca^{2+} currents were further isolated using a *P*/*n* protocol. Series resistance (R_S) measured at the beginning of the perforated- patch recording was 26.3 ± 1.5 MΩ, $n = 15$, for control, and 26.9 ± 1.0 MΩ, $n = 26$, for *dfcr*. For ruptured-patch recordings, R_S was 8.5 ± 0.5 MΩ, $n = 10$, for control, and 10.4 ± 1.3 MΩ, $n = 10$, for *dfcr*. To calculate ΔC_m, the initial 30 ms following the voltage step were ignored due to a non-exocytic capacitance artifact (Neef *et al.* 2007) and the average C_m measured over at least 40 ms. No R_S compensation was used.

Immunofluorescence labelling of mouse organ of Corti

Double-labelling for CtBP2/RIBEYE and GluA2/3 was performed as previously described (Khimich *et al.* 2005). The following antibodies were used: mouse IgG1 anti-CtBP2 (BD Biosciences, 1:200), rabbit anti-GluR2/3 (Chemicon, 1:200) and secondary AlexaFluor488- and AlexaFluor568-labelled antibodies (Molecular Probes, 1:200). Confocal images were acquired using a laser scanning confocal microscope (Leica TCS SP5, Leica MicrosystemsCMS GmbH, Mannheim, Germany) with 488 nm (Ar) and 561 nm (DPSS) lasers for excitation and a ×63 oil immersion objective (NA = 1.4–0.7). For 3-D reconstructions of the specimen, *z*-axis stacks of 2-D images were taken with a step size of 0.5 μm. Image stacks represent maximum *z* projections, done in ImageJ. The CtBP-2/RIBEYE and GluA2/3 immunofluorescence spots were counted in the *z*-stacks and divided by the number of IHCs (number of nuclei in the field of view) in order to yield the number of synapses per IHC. Juxtaposed pre- and postsynaptic spots were considered as mature synapses (Khimich *et al.* 2005).

Results

Harmonin enhances VDF of $Ca_v1.3$ in HEK293T cells

We have previously shown that cotransfection of harmonin with $Ca_v1.3$ channels in HEK293T cells increases ubiquitination of $\alpha_1 1.3$ and decreases

$Ca_v1.3$ current density through enhanced proteosomal degradation of $\alpha_1 1.3$ (Gregory *et al.* 2011). While determining if harmonin affected other parameters of $Ca_v1.3$ function, we noted that harmonin had a particularly prominent effect of enhancing VDF in HEK293T cells. We measured VDF with a triple-pulse voltage protocol in which test current amplitudes are compared before (P1) and after (P2) a conditioning prepulse to various voltages (Fig. 1*A*). Ba^{2+} was used as the charge carrier to increase resolution of VDF by limiting the competing effects of Ca^{2+}-dependent inactivation (CDI). With this protocol, VDF is evident as an increase in the ratio of the P2:P1 current (F_{ratio}) with depolarized prepulse voltages. Cotransfection of harmonin with $Ca_v1.3$ ($\alpha_1 1.3$, β_{1b} and $\alpha_2\delta$ subunits) caused a significant increase in maximal VDF seen with a +50 mV prepulse ($F_{ratio,+50} = 1.18 \pm 0.02$ for $Ca_v1.3$ alone *vs.* 1.52 ± 0.08 for $Ca_v1.3$ + harmonin; $P < 0.01$, by Mann–Whitney rank sum test; Fig. 1*B*). Increased magnitude of I_{Ba} with harmonin was not secondary to shifts in the conductance–voltage profile, since Boltzmann fits of tail current activation curves revealed similar parameters ($V_{1/2} = -19.6 \pm 3.0$; $k = 7.9 \pm 0.8$ for $Ca_v1.3$ alone *vs.* $V_{1/2} = -18.6 \pm 7.5$; $k = 7.6 \pm 1.1$ for $Ca_v1.3$ + harmonin, $P = 0.98$ for $V_{1/2}$ and $P = 0.52$ for k; Fig. 1*C*). These results confirm that harmonin increases $Ca_v1.3$ VDF, which is consistent with its interaction with $Ca_v1.3$ channels in the plasma membrane.

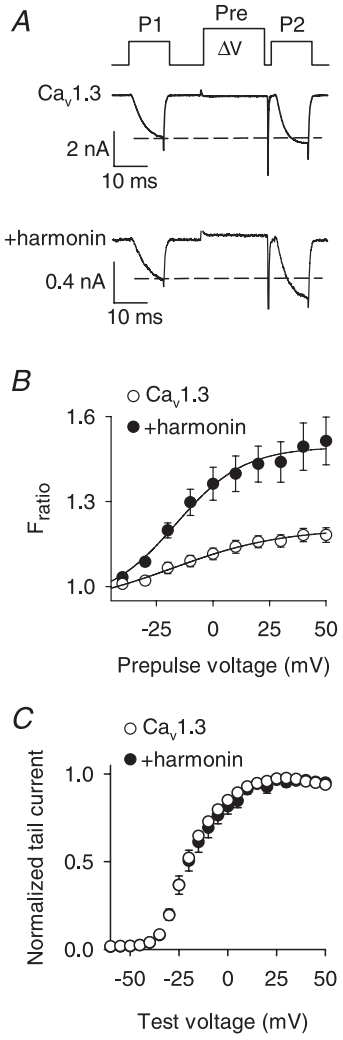

Figure 1. Harmonin enhances VDF of $Ca_v1.3$ channels in transfected HEK293T cells
A, voltage protocol for VDF (top) and representative traces showing I_{Ba} evoked by 10 ms steps from −90 to −20 mV before (P1) and after (P2) a 20 ms conditioning prepulse (Pre) to +50 mV. *B*, ratio of P2/P1 current amplitudes (F_{ratio}) is plotted against prepulse voltage for $Ca_v1.3$ alone ($\alpha_1 1.3$, β_{1b}, $\alpha_2\delta$; $n = 12$) or +harmonin ($n = 12$). *C*, normalized tail current–voltage relationships obtained for $Ca_v1.3$ alone ($n = 14$) or +harmonin ($n = 10$). I_{Ba} was evoked by test pulses from −90 mV to various voltages. Tail currents measured upon repolarization to −70 mV were normalized to the maximal tail current amplitude and plotted against test voltage.

Ca_v β subunits modulate effects of harmonin on $Ca_v1.3$ VDF

Although we found that harmonin modulated the VDF of $Ca_v1.3$ channels containing the auxiliary Ca_v β_{1b} subunit ($Ca_v1.3(\beta_{1b})$, Fig. 1), $Ca_v\beta_2$ is the major $Ca_v\beta$ subunit contributing to $Ca_v1.3$ function in mouse IHCs (Neef *et al.* 2009). Therefore, we characterized the impact of harmonin on VDF in HEK293T cells transfected with $Ca_v1.3$ subunits containing $Ca_v\beta_{2A}$ ($Ca_v1.3(\beta_{2A})$). While $Ca_v1.3(\beta_{2A})$ exhibited marginal VDF ($F_{ratio,+50} = 1.17 \pm 0.02$) that was not significantly different from $Ca_v1.3(\beta_{1b})$ ($F_{ratio,+50} = 1.18 \pm 0.02$; $P = 0.22$, by *t* test; Fig. 2*A*–*C*), cotransfection with harmonin caused a smaller increase in VDF of $Ca_v1.3(\beta_{2A})$ than $Ca_v1.3(\beta_{1b})$. While $Ca_v1.3(\beta_{1b})$ VDF was increased $28.5 \pm 7.2\%$ by harmonin, this increase was only $10.6 \pm 1.6\%$ for $Ca_v1.3(\beta_{2A})$ ($P < 0.05$, by *t* test; Fig. 2*D*). These results confirm the importance of $Ca_v\beta$ subunits in modulating responsiveness of $Ca_v1.3$ VDF to PDZ-domain-containing proteins (Calin-Jageman *et al.* 2007), and suggest that native $Ca_v1.3(\beta_2)$ in IHCs may undergo VDF enhancement by harmonin, although to a lesser extent than $Ca_v1.3(\beta_{1b})$.

Harmonin binding to $\alpha_1 1.3$ dCT is required for VDF enhancement

To test if increased VDF was due to harmonin binding to the $\alpha_1 1.3$ dCT, we took advantage of a short splice variant of the rat $\alpha_1 1.3$ lacking the dCT in which substitution of exon 42A for exon 42 eliminates much of the C-terminal domain including the PDZ-binding sequence in the dCT (Xu & Lipscombe, 2001). We also used $\alpha_1 1.3$ constructs in which the final leucine residue in the

dCT was mutated to alanine ($Ca_v1.3_{L\text{-}A}$; Fig. 3*A*). This mutation disrupts the consensus PDZ-binding sequence and prevents binding of harmonin to a C-terminal fragment of $\alpha_1$1.3 *in vitro* (Gregory *et al.* 2011). To verify that $Ca_v1.3_{42A}$ and $Ca_v1.3_{L\text{-}A}$ have limited interaction with harmonin, we compared their abilities to coimmunoprecipitate with harmonin with that of the wild-type $Ca_v1.3$ in transfected HEK293T cells. While harmonin still coimmunoprecipitated with both $Ca_v1.3_{42A}$ and $Ca_v1.3_{L\text{-}A}$, quantitative analyses revealed a consistent reduction in the amount of harmonin that associated with $Ca_v1.3_{42A}$ and $Ca_v1.3_{L\text{-}A}$ ($66.5 \pm 8.8\%$ and $82.1 \pm 3.9\%$, respectively) compared to wild-type $Ca_v1.3$ (Fig. 3*B* and *C*). Evidently, the dCT contributes to, but is not the sole determinant for, harmonin binding to $Ca_v1.3$. Yet, electrophysiological recordings revealed that $Ca_v1.3_{42A}$ and $Ca_v1.3_{L\text{-}A}$ underwent VDF that was not changed by cotransfection with harmonin. As we have shown previously, $Ca_v1.3_{42A}$ VDF was greater than for exon 42-containing channels, since the dCT contains a module that normally inhibits VDF (Calin-Jageman *et al.* 2007). However, there was no difference in maximal VDF in cells transfected with $Ca_v1.3_{42A}$ alone ($F_{ratio,+50} = 1.37 \pm 0.06$) and those cotransfected with harmonin ($F_{ratio,+50} = 1.44 \pm 0.08$; $P = 0.48$, by *t* test; Fig. 4*A*). Similarly, harmonin did not affect VDF of $Ca_v1.3_{L\text{-}A}$ ($F_{ratio,+50} = 1.14 \pm 0.03$ for $Ca_v1.3_{L\text{-}A}$ alone *vs.* 1.18 ± 0.04 for $Ca_v1.3_{L\text{-}A}$ + harmonin, $P = 0.75$, by *t* test; Fig. 4*B*). These results demonstrate that, despite other potential harmonin interaction sites within the $Ca_v1.3$ channel complex, harmonin binding to the dCT is required for VDF modulation.

The *dfcr* harmonin mutant does not regulate $Ca_v1.3$ VDF

'Deaf-circler' (*dfcr*) mice harbour a mutation in the gene encoding harmonin which deletes 132 amino acids between PDZ domains 2 and 3. Similar to humans with Usher syndrome, *dfcr* mice are deaf and exhibit vestibular defects (Johnson *et al.* 2003). The *dfcr* mutant form of harmonin still contains the PDZ domain 2, which interacts with the $\alpha_1$1.3 dCT, but the internal deletion removes the coiled-coil domain, which disrupts binding of PDZ ligands, including $\alpha_1$1.3 (Gregory *et al.* 2011). The *dfcr* mutant does not bind to the $\alpha_1$1.3 dCT *in vitro* and cannot modulate $Ca_v1.3$ current density like the wild-type harmonin in transfected cells and in mouse IHCs (Gregory *et al.* 2011). Since the effects of the *dfcr* mutant on $Ca_v1.3$ VDF have not been characterized, we first compared the effects of co-transfecting wild-type or *dfcr* harmonin with $Ca_v1.3$ in HEK293T cells.

Consistent with the importance of harmonin interactions with the $\alpha_1$1.3 dCT for modulation of $Ca_v1.3$ VDF (Figs 1–4), *dfcr* harmonin did not augment VDF of $Ca_v1.3(\beta_{2A})$ ($F_{ratio,+50} = 1.15 \pm 0.02$ for $Ca_v1.3(\beta_{2A})$ alone *vs.* 1.14 ± 0.02 for $Ca_v1.3(\beta_{2A})$ + *dfcr*; $P = 0.99$, by *t* test; Fig. 5*A*) or $Ca_v1.3(\beta_{1b})$ ($F_{ratio,+50} = 1.21 \pm 0.02$ for $Ca_v1.3(\beta_{1b})$ alone *vs.* 1.27 ± 0.04 for $Ca_v1.3(\beta_{1b})$ + *dfcr*;

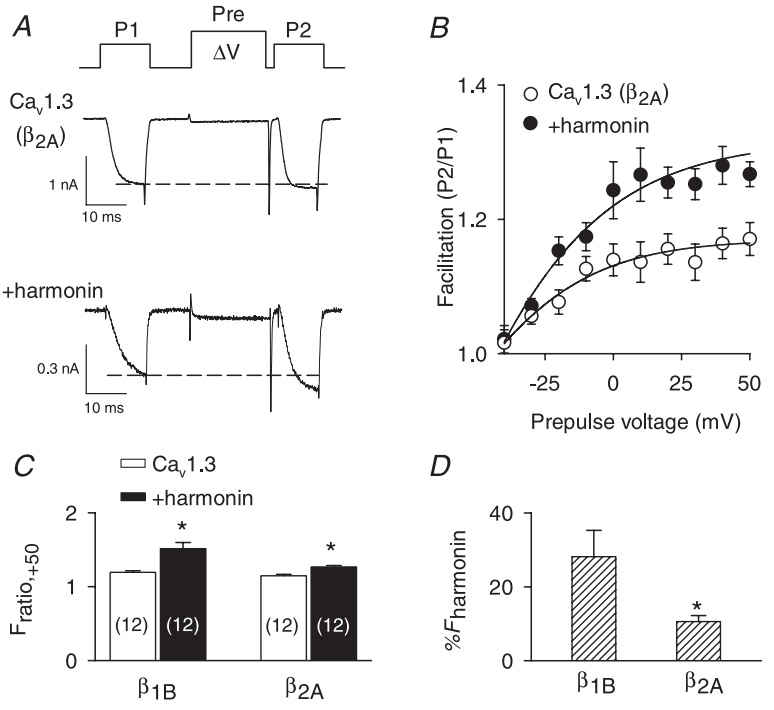

Figure 2. The extent of $Ca_v1.3$ VDF due to harmonin depends on the identity of the $Ca_v\beta$ subunit
A and *B*, voltage protocol, representative I_{Ba}, and F_{ratio} were as described in Fig. 1*A* and *B* except for channels containing the $Ca_v\beta_{2A}$ subunit. $n = 12$ cells for $Ca_v1.3(\beta_{2A})$ alone, $n = 12$ cells for +harmonin. *C*, comparison of facilitation obtained at +50 mV prepulse voltage ($F_{ratio,+50}$) for β_{1b}- or β_{2A}-containing channels. $^*P < 0.001$ compared to $Ca_v1.3$ alone, by *t* test. Number of cells is indicated in parentheses. *D*, percentage increase in $F_{ratio,+50}$ due to harmonin ($\%F_{harmonin}$) for channels with β_{1b} ($n = 12$ cells) or β_{2A} ($n = 12$ cells). $\%F_{harmonin}$ was calculated as ($F_{ratio,+50}$ for $Ca_v1.3$ alone/mean $F_{ratio,+50}$ for +harmonin) × 100. $^*P < 0.05$ by *t* test.

$P = 0.18$, by t test; data not shown). To compare a second metric for VDF, we measured the activation kinetics of I_{Ba} evoked before and after the conditioning prepulse. Since VDF involves enhanced channel opening in response to depolarization, VDF should manifest as faster activation of the P2 current relative to the P1. To test this, we obtained the time constants (τ) for activation with exponential fits of I_{Ba} for P1 and P2, such that enhanced VDF due to harmonin should be measurable as a larger difference in τ for P1 and P2 compared to the *dfcr* mutant ($\Delta\tau$, Fig. 5*B*). While P2 currents activated significantly faster (~36%) than P1 currents in cells cotransfected with harmonin, no such difference was observed with the *dfcr* mutant (Fig. 5*B*). VDF by this metric was significantly greater in cells cotransfected with harmonin than with *dfcr* mutant (~70%; Fig. 5*B*), which further confirms the reduced ability of the *dfcr* mutant to modulate $Ca_v1.3$.

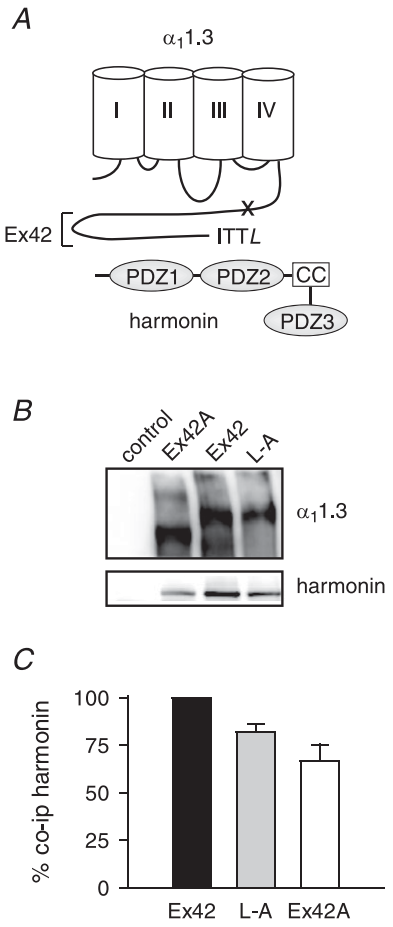

Figure 3. Harmonin binding is reduced by disruption of the PDZ-binding site in the $\alpha_1$1.3 dCT
A, schematic diagram of harmonin and $\alpha_1$1.3. The long C-terminal domain encoded by exon 42 (Ex42) includes the PDZ-binding motif (ITTL) that interacts with the second of three PDZ domains of harmonin. The coiled-coil domain (CC) that is deleted in the *dfcr* harmonin mutant is indicated. The 'x' marks approximate location of truncation of the dCT due to inclusion of exon 42A. *B*, coimmunoprecipitation of harmonin with $Ca_v1.3$ channels in transfected HEK293T cells. Cells were transfected with harmonin alone (control) or cotransfected with $Ca_v1.3$ subunits including $\alpha_1$1.3 with full-length (Ex42) or truncated (Ex42A) dCT or $\alpha_1$1.3 with terminal leucine substituted with alanine (L-A). Western blotting detected $\alpha_1$1.3 (upper panel) and coimmunoprecipitated harmonin (lower panel). *C*, quantification reflecting percentage change in harmonin coimmunoprecipitated with $\alpha_1 1.3_{Ex42A}$ and $\alpha_1 1.3_{L\text{-}A}$ compared to that for $\alpha_1 1.3_{Ex42}$ (%co-ip harmonin). See Methods for details.

Neither wild-type nor *dfcr* harmonin modulate CDI

To determine if harmonin regulates other $Ca_v1.3$ properties in transfected HEK293T cells, we measured the effects of harmonin on inactivation. Like other Ca_v channels, $Ca_v1.3$ undergoes inactivation due to Ca^{2+}- or voltage-dependent mechanisms (CDI or VDI, respectively). CDI is due to calmodulin, which senses local Ca^{2+} influx due to its direct association with the channel (reviewed in Christel & Lee, 2012). Since Ba^{2+} ions bind poorly to calmodulin (Wang, 1985), I_{Ba} exhibits primarily VDI. Depending on the identity of the auxiliary β subunit, I_{Ca} can show both CDI and VDI such that CDI can be isolated as the difference in inactivation of I_{Ca} and I_{Ba}. With 300 ms step-depolarizations, we measured inactivation as the ratio of the residual current amplitude at the end of the pulse (Ires) and the peak current (Ipk) amplitude (I_{res}/I_{pk}), and CDI as the difference in I_{res}/I_{pk} for I_{Ca} and I_{Ba} (Fig. 6*A*). As expected, I_{Ca} inactivated significantly faster than I_{Ba} in cells transfected with $Ca_v1.3$ alone or cotransfected with harmonin or the *dfcr* mutant. However, there was no difference in CDI between the three groups (Fig. 6*A*). Since our metric for CDI may not have detected effects of harmonin or *dfcr* on the kinetics of CDI, we compared parameters from double exponential fits of the I_{Ca}. There was no significant difference in the fractional contribution or time constants for fast or slow inactivation (Fig. 6*B*). These results indicate that harmonin does not affect CDI in transfected HEK293T cells.

Impaired VDF in a mouse model of Usher syndrome

To test the physiological relevance of $Ca_v1.3$ VDF modulation by harmonin, we performed whole-cell patch clamp recordings of IHCs from mice expressing the *dfcr* mutant. We showed previously that $Ca_v1.3$ current density is abnormally elevated in IHCs from mature *dfcr* mice, consistent with decreased proteosomal degradation of $Ca_v1.3$ (Gregory *et al.* 2011). If harmonin also enhances VDF of $Ca_v1.3$, we would expect VDF to be reduced in IHCs from *dfcr* mice. Since the presynaptic localization of harmonin and functional interactions of harmonin with $Ca_v1.3$ are characteristic of IHCs from mice at ages (older than p12) after hearing onset (Gregory *et al.* 2011),

modulation of $Ca_v1.3$ VDF would be expected in mouse IHCs at p16–18 but not p6–8.

To test these predictions, we compared $Ca_v1.3$ VDF in IHCs from heterozygous control and homozygous mutant *dfcr* mice. Since $Ca_v1.3$ accounts for ∼90% of the IHC whole-cell Ca^{2+} current (Platzer *et al.* 2000; Brandt *et al.* 2003), recording solutions were designed to isolate $Ca_v1.3$ I_{Ba} from other ionic currents without the addition of Ca_v channel blockers. To determine the optimal conditions for measuring VDF in IHCs, we measured the onset of VDF by comparing test currents evoked before (P1) and after (P2) a conditioning prepulse of varying durations. VDF increased exponentially with prepulse duration with a time constant of ∼11 ms (Fig. 7*A*). Since maximal VDF was obtained with a 50 ms prepulse duration, we used 50 ms prepulses for the comparisons of VDF in control and *dfcr* IHCs. Consistent with our findings in HEK293T cells, I_{Ba} exhibited modest VDF in mature (p16–18) control IHCs ($F_{ratio,+50} = 1.15 \pm 0.01$) that was significantly weaker in IHCs from *dfcr* mice ($F_{ratio,+50} = 1.07 \pm 0.01$, $P < 001$, by *t* test; Fig. 7*B*). This difference in VDF was not observed in immature IHCs (p6–8; $F_{ratio,+50} = 1.08 \pm 0.01$ for control *vs.* 1.07 ± 0.01 for *dfcr*, $P = 0.59$, by *t* test; Fig. 7*C*). VDF in mature IHCs was associated with significantly faster activation kinetics of I_{Ba} evoked after (P2) compared to before (P1) the prepulse (in control IHCs, $\tau_{P1} = 0.60 \pm 0.04$ ms *vs.* $\tau_{P2} = 0.37 \pm 0.02$ ms for +50 mV prepulse; $P < 0.001$, by paired *t* test; Fig. 8*A* and *B*). By this metric, VDF was still evident in *dfcr* IHCs ($\tau_{P1} = 0.66 \pm 0.05$ ms *vs.* $\tau_{P2} = 0.41 \pm 0.03$ ms for +50 mV prepulse; $P < 0.001$, by paired *t* test; Fig. 8*C*). However, in *dfcr* IHCs, the prepulse-induced acceleration of I_{Ba} activation was 30–68% weaker than in control IHCs ($\Delta\tau = 0.11 \pm 0.02$ ms for control *vs.* 0.05 ± 0.01 ms for *dfcr*, $P = 0.02$ by Mann–Whitney rank sum test; Fig. 8*D*). Reduced VDF in mature *dfcr* IHCs was not secondary to differences in control and *dfcr* IHCs in terms of CDI or VDI (Supplemental Fig. 1, available online only), or voltage-dependent activation of I_{Ba} (Table 1). Therefore, in addition to regulating $Ca_v1.3$ channel density in the plasma membrane, harmonin also potentiates $Ca_v1.3$ VDF in mature mouse IHCs.

We next evaluated modulation of VDF by harmonin using Ca^{2+} as the charge carrier. We combined whole-cell patch-clamp recordings of total I_{Ca} in the plasma membrane and fast confocal Ca^{2+} imaging of individual IHC active zones (Frank *et al.* 2009; Gregory *et al.* 2011). With this approach, we found a small but significant VDF of the P2 relative to the P1 peak I_{Ca} and charge integral (Table 2) in control and *dfcr* IHCs, without any significant difference between the genotypes. As shown previously (Gregory *et al.* 2011), the amplitude of presynaptic Ca^{2+} microdomains was significantly elevated in *dfcr* compared to control IHCs (baseline-normalized

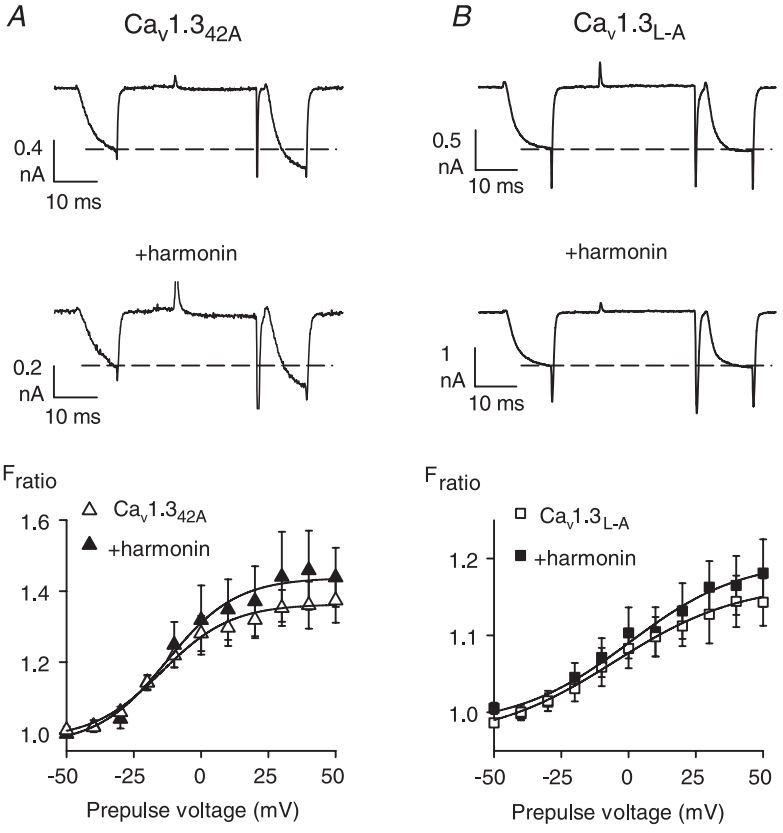

Figure 4. Disruption of the PDZ-binding site in $\alpha_1$1.3 prevents modulation of VDF by harmonin
Same as in Fig. 1*A* and *B* except for cells transfected with $Ca_v1.3_{42A}$ alone ($n = 10$) or +harmonin ($n = 6$) (*A*), or $Ca_v1.3_{L\text{-}A}$ alone ($n = 12$) or +harmonin ($n = 9$) (*B*).

fluorescence change $\Delta F/F_0$, Table 2). While the $\Delta F/F_0$ amplitude did not increase following the conditioning pulse, the Ca^{2+} microdomains build-up tended to be faster in response to P2 compared to the P1 test pulse indicating the presence of modest VDF. The difference in kinetics of P1 and P2 signals did not reach statistical significance, perhaps related to the slower time course of the active zone Ca^{2+} signals (τ_{P1} ~2 ms) compared to whole-cell measurements of I_{Ba} (τ_{P1} ~0.6 ms). While multiple factors could hinder detection of differences in VDF of whole-cell I_{Ca} and synaptic Ca^{2+} signals in control and *dfcr* IHCs (see Discussion), these results demonstrate that VDF is a feature of $Ca_v1.3$ channels in IHCs using Ca^{2+} as the permeant ion.

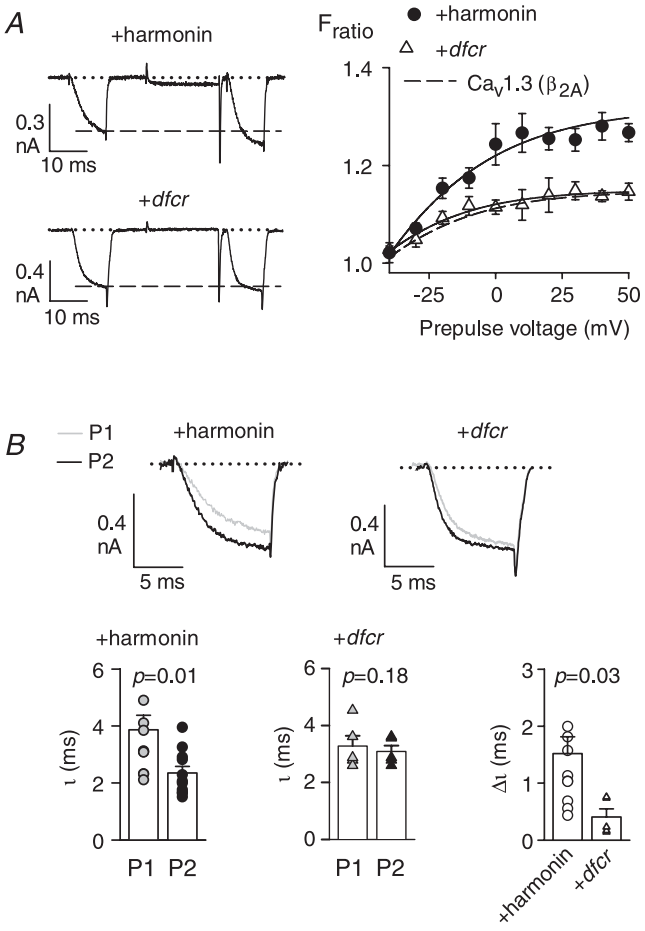

Figure 5. The *dfcr* mutant of harmonin does not enhance $Ca_v1.3$ VDF
A, same as in Fig. 1*A* and *B* except for cells transfected with $Ca_v1.3(\beta_{2A})$ alone ($n = 12$) or +*dfcr* ($n = 5$). Dashed line in graph represents data redrawn from Fig. 2*B* for $Ca_v1.3(\beta_{2A})$ + harmonin. *B*: top, representative current traces for P1 and P2 overlaid for comparison; bottom, time constants measured from exponential fits of P1 or P2 current traces for $Ca_v1.3(\beta_{2A})$ + harmonin or $Ca_v1.3(\beta_{2A})$ + *dfcr*. $\Delta\tau$ represents difference in τ for P1 and P2 currents. *P* values for τ were determined by *t* test and for $\Delta\tau$ from paired *t* test.

Impaired exocytosis in *dfcr* IHCs

$Ca_v1.3$ mediates stimulus–secretion coupling in IHCs (Platzer *et al.* 2000; Brandt *et al.* 2003), whereby exocytosis of a synaptic vesicle may be controlled by few $Ca_v1.3$ channels within nanometer proximity (Brandt *et al.* 2005). Compared to wild-type harmonin, the *dfcr* mutant causes abnormally high $Ca_V1.3$ current density (Gregory *et al.* 2011) and reduced VDF (Figs 7 and 8), which could have dual, and potentially complex, effects on IHC exocytosis. To gain insight into the functional consequences of the *dfcr* mutation on IHC exocytosis, we performed perforated-patch (Fig. 9*A–D*) and ruptured-patch (Fig. 9*E–H*) recordings of membrane capacitance changes (ΔC_m) evoked by step depolarizations. The test voltage evoking the maximal I_{Ca} was determined in current–voltage (*I–V*) relations (Fig. 9*A* and *E*). Interestingly, Boltzmann fits of the *I–V* curves for I_{Ca} revealed a small but significant negative shift in the half-maximal activation voltage for *dfcr* compared to control IHCs both in perforated-patch and

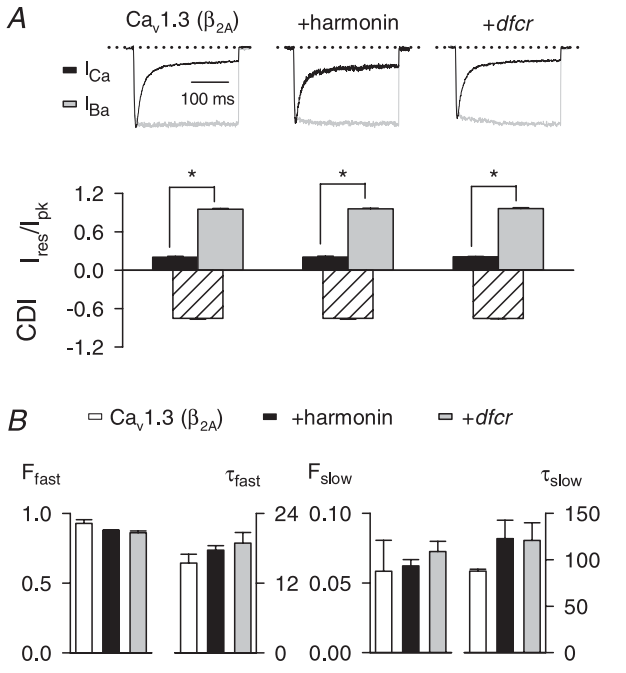

Figure 6. $Ca_v1.3$ CDI is not affected by harmonin or the *dfcr* mutant
A, top, representative traces for I_{Ca} and I_{Ba} normalized and overlaid for comparison in cells transfected with $Ca_v1.3(\beta_{2A})$ alone or cotransfected with harmonin or *dfcr*. Currents were evoked by 300 ms pulses to −20 mV from −90 mV. Bottom, inactivation was calculated as the current amplitude at the end of the pulse normalized to the peak current amplitude (I_{res}/I_{pk}) and is shown for I_{Ca} and I_{Ba}. CDI represents the difference in I_{res}/I_{pk} for I_{Ca} and the mean I_{res}/I_{pk} for I_{Ba}. For $Ca_v1.3(\beta_{2A})$ alone, $n = 5$ for I_{Ca}, $n = 10$ for I_{Ba}; for +harmonin, $n = 7$ for I_{Ca}, $n = 11$ for I_{Ba}; for +*dfcr*, $n = 9$ for I_{Ca}, $n = 9$ for I_{Ba}. $^*P < 0.001$ by *t* test. *B*, parameters obtained from double exponential fits of current traces obtained as in *A*.

ruptured-patch recordings, which was not observed for I_{Ba} (Table 1). The increased $Ca_v1.3$ current density in *dfcr* IHCs was less apparent than reported previously (Gregory *et al.* 2011), perhaps due to the larger age range of mice in these experiments (p13–20 *vs.* p16–18). With a 20 ms step to elicit maximal I_{Ca} in each cell, ΔC_m was significantly reduced in *dfcr* compared to control IHCs (Fig. 9*B*).

Previous work has demonstrated the existence of distinct populations of exocytic vesicles that differ in release kinetics and Ca^{2+} dependence. A readily releasable pool (RRP) of vesicles undergoes fast, synchronous exocytosis and is efficiently recruited by short (10–20 ms) stimuli. A slower phase of exocytosis is observed during sustained depolarizations (Moser & Beutner, 2000; Goutman & Glowatzki, 2007). To further characterize the exocytic defect in *dfcr* IHCs, we compared ΔC_m evoked by varying stimulus durations. With short (10–20 ms) depolarizing pulses, ΔC_m was significantly reduced in *dfcr* compared to control IHCs (~41%, $P < 0.007$ for 10 ms pulses, ~36%, $P = 0.011$ for 20 ms pulses; Fig. 9*C*), while there was no difference in ΔC_m evoked by longer (50–100 ms) depolarizations ($P = 0.85$ for 50 ms, $P = 0.49$ for 100 ms by Wilcoxon rank test; Fig. 9*C*). These results suggested impairment in synchronous exocytosis of the RRP in *dfcr* IHCs. Harmonin-dependent VDF may enhance rapid Ca^{2+} signalling at active zones in control IHCs. If so, then the difference in ΔC_m in *dfcr* and control IHCs should be eliminated upon normalizing ΔC_m to the charge integral of I_{Ca} ($\Delta C_m/Q_{Ca}$). By this analysis, maximal efficiency of exocytosis was ~3 fF pC^{-1} (Fig. 9*D*), similar to that reported in frog auditory hair cells (Graydon *et al.* 2011). $\Delta C_m/Q_{Ca}$ was still significantly smaller in *dfcr* compared to control IHCs (Fig. 9*D*), which suggested a reduced efficiency of Ca^{2+} influx for driving exocytosis in *dfcr* compared to control IHCs.

To follow up this possibility, we performed whole-cell patch clamp measurements of ΔC_m including EGTA (4 mM + 2 mM Ca^{2+}, calculated free intracellular $[Ca^{2+}] = 106$ nM) in the intracellular recording solution. As a slow Ca^{2+} buffer, EGTA affects sustained exocytosis more strongly than RRP exocytosis, which probably reflects a requirement for long-distance Ca^{2+} signalling involved in replenishment of depleted vesicles (Moser & Beutner, 2000). If there was looser spatial coupling of

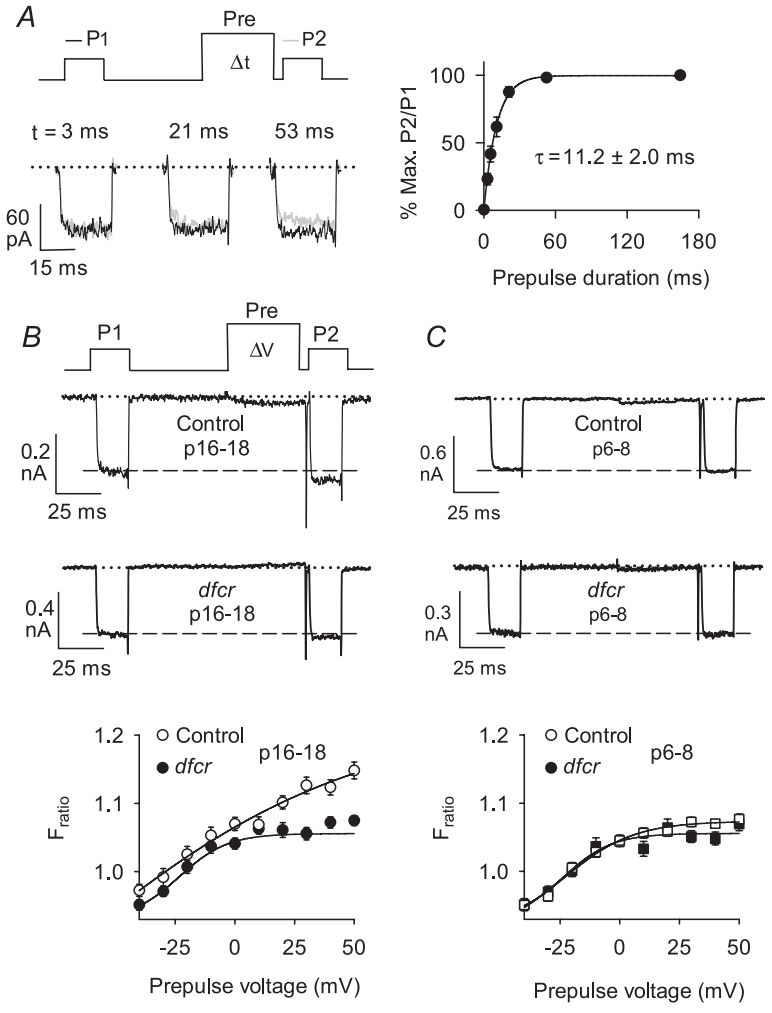

Figure 7. VDF is weaker in *dfcr* compared to control IHCs after hearing onset in mice
A, measurement of VDF onset. Left, voltage protocol and representative current traces obtained with indicated prepulse durations. P1 and P2 currents are overlaid for comparison. Right, P2/P1 ratios were expressed as percentage of the maximal VDF obtained with a 165 ms prepulse and plotted against prepulse duration. Smooth line represents single-exponential fit. The mean time constant (±SEM) is indicated. *B* and *C*, top, voltage protocol for IHC VDF showing 20 ms test pulses (P1, P2) from −75 to −15 mV separated by a 50 ms prepulse to various voltages. Representative traces for I_{Ba} obtained with +50 mV prepulse for IHCs from postnatal days (p) 16–18 (*B*) or p6–8 (*C*) control ($n = 25$ for p16–18, $n = 18$ for p6–8) or *dfcr* ($n = 26$ for p16–18, $n = 18$ for p6–8) mice. Dashed line represents initial amplitude of P1 current. Bottom, F_{ratio} was calculated as P2 divided by P1 current amplitude and plotted against prepulse voltage.

$Ca_v1.3$ channels and RRP vesicles in *dfcr* compared to control IHCs, we would expect a stronger effect of EGTA on synchronous exocytosis in *dfcr* IHCs than in control IHCs. However, with EGTA in ruptured-patch recordings, we found RRP exocytosis of *dfcr* IHCs to be more similar to control IHCs (Fig. 9*G*) than in perforated-patch recordings. $\Delta C_m/Q_{Ca}$ still tended to be smaller in *dfcr* than in control IHCs with EGTA (Fig. 9*H*), although not quite reaching statistical significance ($P = 0.053$ comparing *dfcr vs.* control $\Delta C_m/Q_{Ca}$ response to 20 ms depolarization in ruptured patch). There was no significant difference in *dfcr* IHCs in $\Delta C_m/Q_{Ca}$ evoked by 20 ms depolarizations in ruptured-patch or perforated-patch recordings ($P = 0.12$; Fig. 9*D* and *H*). These results argue against a looser spatial coupling of the RRP to $Ca_v1.3$ channels in *dfcr* IHCs.

To determine if smaller numbers of IHC synapses could contribute to the exocytic impairment in *dfcr* IHCs, we quantified afferent IHC synapses in stacks of confocal sections from organs of Corti immunolabelled for presynaptic ribbons (CtBP2/RIBEYE) and postsynaptic AMPA glutamate receptors (GluA2/3; Khimich *et al.* 2005). However, there was no significant difference between control and *dfcr* IHCs in the cochlear apex (8.5 ± 0.6 for control, $n = 85$ cells *vs.* 9.7 ± 0.4 for *dfcr*, $n = 49$ cells; $P = 0.2$ by *t* test). These results suggest that the exocytic defect in *dfcr* IHCs does not involve changes in synapse number, but could depend on pre-synaptic alterations in RRP dynamics at the subset of synapses characterized by harmonin/$Ca_v1.3$ interactions. Our results indicate a multi-faceted role of harmonin in regulating $Ca_v1.3$ channel function and RRP exocytosis in mature IHCs, both of which are compromised in the *dfcr* model of Usher syndrome.

Table 1. *I–V* parameters for I_{Ca} and I_{Ba} in control and *dfcr* IHCs

I_{Ba} (whole-cell)	Control ($n = 43$)	*dfcr* ($n = 41$)	*P* value
G (nS)	7.5 ± 0.5	7.0 ± 0.5	0.49
$V_{1/2}$ (mV)	−18.2 ± 0.6	−19.1 ± 0.7	0.30
E (mV)	48.9 ± 1.0	49.1 ± 1.0	0.91
k	6.4 ± 0.2	6.3 ± 0.2	0.57
I_{Ca} (whole-cell)	Control ($n = 11$)	*dfcr* ($n = 13$)	*P* value
G (nS)	5.41 ± 0.19	5.86 ± 0.37	0.30
$V_{1/2}$ (mV)	−21.4 ± 0.8	−26.1 ± 1.0	0.002
E (mV)	43.4 ± 0.8	43.3 ± 0.6	0.94
k	6.7 ± 0.3	7.3 ± 0.3	0.26
I_{Ca} (perforated-patch)	Control ($n = 22$)	*dfcr* ($n = 40$)	*P* value
G (nS)	5.91 ± 0.25	5.98 ± 0.28	0.87
$V_{1/2}$ (mV)	−24.3 ± 0.7	−27.9 ± 0.5	< 0.001
E (mV)	49.6 ± 1.12	47.8 ± 0.8	0.20
k	4.7 ± 0.2	4.6 ± 0.2	0.71

I_{Ba} and I_{Ca} were recorded in whole-cell (ruptured patch) or perforated-patch configuration and analysed as described in Methods. I-V relationships were fit with the following equation: $I = G(V - E)/\{1 + \exp[(V_{1/2} - V)/k]\}$ where *G* is conductance, *V* is test potential, *E* is apparent reversal potential, $V_{1/2}$ is potential of half activation, *k* is the slope factor. Values represent mean ± SEM. *n* represents number of IHCs analysed. *P* values were obtained from unpaired *t* tests or Wilcoxon rank test.

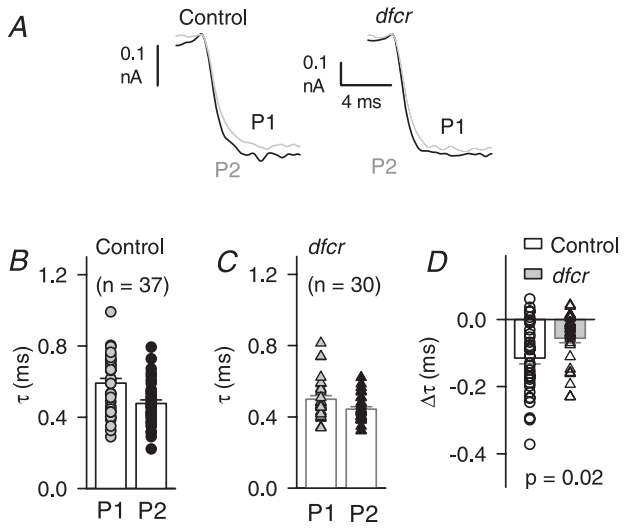

Figure 8. VDF accelerates I_{Ba} activation to a greater extent in control than in *dfcr* IHCs
A, voltage protocol and representative traces for P1 and P2 currents overlaid for comparison of activation kinetics. Results are shown from IHCs from p16–18 control or *dfcr* mice. *B* and *C*, time constant (τ) from exponential fit of the rising phase of P1 and P2 I_{Ba} traces as shown in *A* from control ($n = 37$, *B*) and *dfcr* ($n = 30$, *C*) IHCs. Symbols represent values from individual cells, bars represent mean ± SEM. *D*, acceleration in activation due to VDF measured as the difference in τ for P1 and P2 ($\Delta\tau$) measured as in *B* for control and *dfcr* IHCs. *P* value determined by *t* test.

Discussion

Our study provides multiple new insights into the regulation of $Ca_v1.3$ channels by harmonin. First, harmonin binding to the distal C-terminus of $\alpha_1 1.3$ enhances VDF of $Ca_v1.3$ current, the extent to which depends on the identity of the $Ca_v\beta$ subunit. Second, in mouse IHCs, VDF characterizes $Ca_v1.3$ currents after, but not before, hearing onset and potentiates presynaptic $Ca_v1.3$ currents by accelerating $Ca_v1.3$ activation kinetics. Third, $Ca_v1.3$ VDF and exocytosis are impaired in IHCs from *dfcr* mice expressing a mutant form of harmonin. We conclude that harmonin is an important determinant of $Ca_v1.3$ properties and presynaptic function in mouse IHCs.

Dual regulation of $Ca_v1.3$ channels by harmonin

Facilitation of Ca_v1 channels occurs by multiple mechanisms that have been studied extensively in the

Table 2. VDF probed by whole-cell patch clamp recording and Ca^{2+} imaging at active zones

	Control ($n = 41$ spots, 14 IHCs)	*dfcr* ($n = 41$ spots, 16 IHCs)	*P* value
VDF (I_{Ca})	2.9 ± 1.1%	3.2 ± 0.7%	0.79 (ut)
I_{Ca} (P1) *vs.* I_{Ca} (P2)	$P = 0.003$ (pt)	$P = 0.0004$ (pt)	
VDF (Q_{Ca})	1.2 ± 0.6%	2.0 ± 0.6%	0.16 (w)
Q_{Ca} (P1) *vs.* Q_{Ca} (P2)	$P = 0.045$ (pt)	$P = 0.002$ (pt)	
$\Delta F/F_0$ (P1)	0.64 ± 0.36	0.98 ± 0.84	0.02 (w)
$\Delta F/F_0$ (P2)	0.62 ± 0.34	0.95 ± 0.79	0.01 (w)
$\tau_{\Delta F,P1}$	1.6 ± 0.5 ms	1.8 ± 0.6 ms	0.40 (w)
$\tau_{\Delta F,P2}$	1.5 ± 0.4 ms	1.7 ± 0.5 ms	0.13 (w)

Whole-cell Ca^{2+} currents (I_{Ca}) were elicited by 20 ms test pulses (to −32 mV) before (P1) and after (P2) a 50 ms prepulse (to +63 mV) in control and *dfcr* IHCs. VDF of I_{Ca} was calculated as the percentage increase in the peak amplitude (VDF (I_{Ca})) or the current integral (VDF (Q_{Ca})) of I_{Ca} evoked by the P2 pulse compared to the P1 pulse. Data represent mean ± SEM. Ca^{2+} influx at individual active zones of these cells was approximated by the change in fluorescence of the low affinity Ca^{2+} indicator Fluo-5N (background-subtracted and normalized; $\Delta F/F_0$). Time constants corresponding to the rise in Ca^{2+} derived from single exponential fitting to the depolarization-evoked ΔF ($\tau_{\Delta F,P1}$ for P1; $\tau_{\Delta F,P2}$ for P2). Data represent mean ± SD. $[Ca^{2+}]_i$ was 5 mM in these experiments to better resolve $\Delta F/F_0$. The present analysis was performed on data extracted from the same recordings performed in a previous study in which effects of the *dfcr* mutation on only the P1 (control) current were reported (Gregory *et al.* 2011). Data were tested for randomness, normal distribution and equality of variances, then appropriate statistical tests were chosen (pt, paired *t* test; ut, unpaired *t* test; w, Wilcoxon rank test).

context of nerve and muscle (Dolphin, 1996). VDF has been reported for $Ca_v1.3$ channels in transformed cell lines (Safa *et al.* 2001; Calin-Jageman *et al.* 2007), neonatal mouse outer hair cells (Michna *et al.* 2003), and mouse sinoatrial nodal cells in the heart (Christel *et al.* 2012). Our results provide the first evidence that $Ca_v1.3$ channels in IHCs undergo VDF and that harmonin contributes to this process. The mechanism involves harmonin binding to the PDZ-binding sequence in the $\alpha_1$1.3 dCT, since mutation or deletion of this motif prevents modulation of VDF (Fig. 4). In addition, the *dfcr* mutant, which cannot bind the $\alpha_1$1.3 dCT (Gregory *et al.* 2011) does not enhance VDF (Fig. 5). Similar to the PDZ protein erbin, binding of harmonin to the $\alpha_1$1.3 dCT may relieve an autoinhibitory regulation of VDF imposed by the $\alpha_1$1.3 dCT (Calin-Jageman *et al.* 2007). However, harmonin binding to the $\alpha_1$1.3 dCT also promotes ubiquitination of $\alpha_1$1.3, which limits $Ca_v1.3$ current density by promoting proteosomal degradation of the channel (Gregory *et al.* 2011). Harmonin may dually regulate $Ca_v1.3$ channels by limiting channel trafficking to, or enhancing removal from, the plasma membrane through targeting to proteosomal pathways. Those channels that remain associated with harmonin at the IHC synapse exhibit enhanced VDF due to the $\alpha_1$1.3 dCT interaction. Our findings that $Ca_v1.3$ current density is increased (Gregory *et al.* 2011) and VDF is decreased (Figs 7 and 8) in IHCs from *dfcr* compared to control mice support the bifunctional role of harmonin with respect to $Ca_v1.3$ regulation *in vivo*. Our coimmunoprecipitation experiments suggest that harmonin may interact with sites in the channel complex in addition to the dCT (Fig. 3), raising the possibility that harmonin may regulate yet other aspects of $Ca_v1.3$ function.

VDF in HEK293T cells cotransfected with $Ca_v1.3$ and harmonin (Figs 1*B* and 2*B*) was stronger and occurred at more negative potentials compared to VDF in control IHCs (Fig. 7*B*). A contributing factor is that VDF is somewhat limited in $Ca_v1.3$ channels containing the β_2 subunit (Fig. 2*C* and *D*), which is the primary $Ca_v\beta$ subunit in mouse IHCs (Neef *et al.* 2009). In addition, harmonin is found at only ∼50% of mature IHC synapses, whereas $Ca_v1.3$ is present at every synapse (Brandt *et al.* 2005; Gregory *et al.* 2011). Since our whole-cell recordings summate the activity of all IHC $Ca_v1.3$ channels, the impact of harmonin on VDF would be diluted by the nominal VDF exhibited by channels not associated with harmonin. Considering the proportion of harmonin-positive synapses in mature IHCs (∼50%), the ∼13% increase in I_{Ba} amplitude due to a +30 mV prepulse in mature IHCs VDF may be twice as large at individual synapses characterized by $Ca_v1.3$/harmonin interactions and thus roughly similar to what we find for $Ca_v\beta_2$-containing channels in HEK293T cells (∼25% for a +30 mV prepulse; Fig. 2*B*).

Considering the above argument, our inability to measure harmonin-dependent VDF using Ca^{2+} as the charge carrier, both in electrophysiological recordings of I_{Ca} and Ca^{2+} imaging of presynaptic active zones is not unexpected (Table 2). Moreover, VDF of I_{Ca} in IHCs is likely to be further diminished by CDI. While not as prominent for $Ca_v1.3$ in transfected HEK293T cells as in IHCs (compare Fig. 6 and Supplemental Fig. 1), CDI is still fast enough in IHCs (τ_{fast} ∼5–7 ms, Supplemental Fig. 1) to partially occlude VDF (τ ∼11 ms, Fig. 7*A*) in whole-cell recordings. Given these caveats, we propose that VDF is physiologically relevant for controlling I_{Ca} at the subset of synapses characterized by $Ca_v1.3$/harmonin interactions in mature IHCs.

Physiological significance of $Ca_v1.3$ VDF in IHCs

VDF due to harmonin is measurable in mature IHCs but not in IHCs prior to hearing onset (Fig. 7*B*), which coincides with the developmental upregulation of harmonin localization at IHC synapses (Gregory *et al.* 2011). At very positive voltages (+50 mV), VDF causes ∼20% acceleration in the activation rate of the

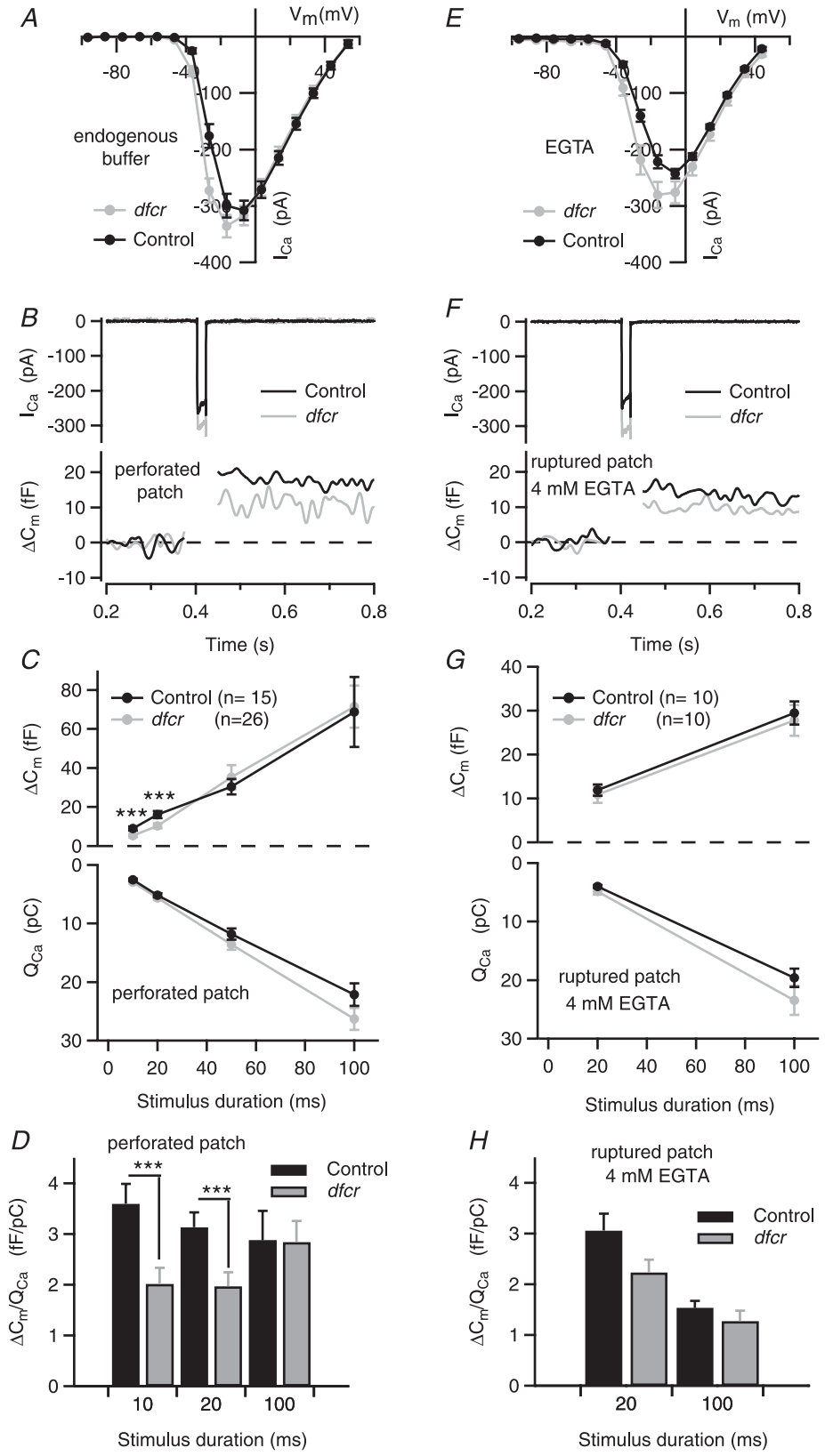

Figure 9. Presynaptic function is altered in *dfcr* IHCs
I_{Ca} and exocytic membrane capacitance changes (ΔC_m) were measured in perforated-patch (*A–D*) and ruptured-patch configurations (4 mM EGTA + 2 mM Ca^{2+} in the pipette, *E–H*). The extracellular Ca^{2+} was

macroscopic $Ca_v1.3$ current (Fig. 8*B*), an effect that could be twice as large at harmonin-positive synapses. Consistent with this possibility, VDF due to a +50 mV prepulse caused a ∼36% speeding of I_{Ba} activation in HEK293T cells cotransfected with $Ca_v1.3$ and harmonin (Fig. 5*B*). Facilitation of I_{Ca} in response to prior depolarization has been reported for I_{Ca} at rat IHC synapses (Goutman & Glowatzki, 2011; Goutman, 2012) and at retinal bipolar synapses (Cho & von Gersdorff, 2012) and so may be a fundamental form of Ca_v1 regulation at ribbon synapses.

Exocytosis of the RRP is triggered by the opening of relatively few $Ca_v1.3$ channels (Brandt *et al.* 2005) such that changes in the microscopic properties of $Ca_v1.3$ may substantially affect transmitter release. In this respect, modulation of $Ca_v1.3$ gating by harmonin is consistent with the impairment of synchronous exocytosis in *dfcr* IHCs (Fig. 9). By amplifying presynaptic $Ca_v1.3$ influx as a function of membrane depolarization, VDF could also contribute to short-term facilitation of IHC transmission. This form of presynaptic plasticity has been documented in afferent recordings at synapses of frog auditory hair cells (Cho *et al.* 2011) and rat IHCs, where it manifests as a decrease in synaptic failures and delays following pre-depolarizations (Goutman & Glowatzki, 2011). Ca^{2+} current facilitation in the latter study on immature IHCs was relatively modest and not thought to significantly contribute to the synaptic facilitation, which could be due to the decreased localization of harmonin at immature IHC synapses (Gregory *et al.*, 2011). Thus, at select harmonin-positive IHC synapses, $Ca_v1.3$ VDF may increase the gain and enhance the timing of release events, thus improving aspects of intensity and temporal coding of sound, respectively. Maintaining $Ca_v1.3$ channel availability during graded changes in the IHC membrane potential is important for the continuous encoding of sound information (Lewis & Hudspeth, 1983; Moser *et al.* 2006) as well as for ongoing spontaneous afferent firing (Robertson & Paki, 2002; Sueta *et al.* 2004). Although $Ca_v1.3$ channels show less inactivation (both CDI and VDI) in IHCs compared to other cell types (Platzer *et al.* 2000; Koschak *et al.* 2001), CDI and VDI are still measurable and can, along with RRP depletion (Moser & Beutner, 2000), lead to significant synaptic depression if unopposed (Cho *et al.* 2011).

A role for harmonin in synchronous exocytosis

Based on our findings that Ca^{2+} influx–exocytosis coupling is impaired in *dfcr* IHCs, we expected that intracellular dialysis with EGTA in whole-cell recordings should more strongly inhibit RRP exocytosis in *dfcr* IHCs compared to control IHCs, which was not the case (Fig. 9). This result could be explained by a role for harmonin in regulating Ca^{2+} coupling to only one component of the RRP, which could not be resolved in our measurements of ΔC_m. While paired pre- and postsynaptic recordings of synaptic transmitter release indicate two components of the RRP (Wu & Borst, 1999; Sakaba & Neher, 2001; Goutman & Glowatzki, 2007; but see Li *et al.* 2009), only one RRP was reported with ΔC_m measurements of exocytosis (Moser & Beutner, 2000). Thus, our ΔC_m recordings may have lacked the sensitivity to detect a stronger effect of EGTA on RRP exocytosis in *dfcr* IHCs when compared to control, which would further be challenged by an effect of harmonin at only a subset of IHC active zones (Gregory *et al.* 2011).

Alterations in exocytosis in *dfcr* IHCs could suggest additional synaptic functions of harmonin that may be independent of $Ca_v1.3$ modulation. Analogous to its properties in apical IHC hair bundles (Adato *et al.* 2005), harmonin could engage in multivalent interactions with $Ca_v1.3$ channels and/or other synaptic molecules that could regulate Ca^{2+} coupling to exocytosis in IHCs. For example, harmonin, either alone or in complex with cadherin-23, binds to phosphatidylinositol 4,5-bisphosphate (PIP_2) (Bahloul *et al.* 2010). PIP_2 is a known regulator of exocytosis in other cell types (Koch & Holt, 2012) and reductions in PIP_2 synthesis causes defects in Ca^{2+} signalling and high-frequency hearing-impairment mice (Rodriguez *et al.* 2012). A detailed understanding of the molecular mechanism by which harmonin regulates the Ca^{2+} efficiency of

10 mM to adequately resolve ΔC_m. *A*, *I–V* relationship for I_{Ca} evoked by 10 ms voltage steps from −96.6 mV in perforated-patch recordings (control: $n = 23$, *dfcr*: $n = 40$). *B*, representative I_{Ca} and ΔC_m (C_m filtered at 50 Hz) in response to 20 ms depolarization to voltage eliciting peak I_{Ca}. *C*, ΔC_m (top) and corresponding I_{Ca} integral (Q_{Ca}, bottom) in response to step pulses for the indicated durations. Depolarizations were from −96.6 mV to the voltage eliciting peak I_{Ca} (between −26.6 and −16.6 mV) for each cell. Data represent grand averages (calculated from the means of the individual cells, $n = 26$ for *dfcr* and 15 for control IHCs (p13–19) ± SEM. *D*, reduced Ca^{2+} efficiency of synchronous exocytosis in *dfcr* IHCs in response to depolarizations eliciting peak I_{Ca} in perforated-patch recordings. ΔC_m was normalized to Q_{Ca} obtained with different stimulus durations in *B* and *C* and shown for control and *dfcr* IHCs (***$P < 0.01$, by Student's *t* test). *E*, *I–V* relationship for I_{Ca} evoked by 10 ms voltage steps from −96.2 mV (control: $n = 11$, *dfcr*: $n = 13$) in ruptured-patch recordings. *F* and *G*, same as in *B* and *C*, but for data obtained with ruptured-patch configuration with 4 mM EGTA and 2 mM Ca^{2+} in the intracellular solution. In *F*, $n = 10$ for *dfcr* and 10 for control IHCs. *G* and *H*, tendency towards reduced Ca^{2+} efficiency of synchronous exocytosis was also observed in EGTA-loaded *dfcr* IHCs. *H*, same as in *D*, but for ruptured-patch configuration ($n = 10$ for control, $n = 10$ for *dfcr*).

exocytosis will require more in-depth analyses, such as paired recordings of IHCs and postsynaptic afferents in genetically modified mice.

A presynaptic role for harmonin in IHCs

In apical hair bundles, the role of harmonin has been elegantly elucidated. The PDZ domains of harmonin bind to multiple proteins (sans, myosin VIIa, cadherin-23) implicated in hair bundle development (Adato *et al.* 2005). Mutations in harmonin or these interacting proteins cause deafness in humans with Usher syndrome and animal models (Petit, 2001), due to improper formation of hair bundles and subsequent failure of mechanotransduction. In *dfcr* mice, hair bundles of IHCs are grossly normal (Grillet *et al.* 2009), but mechanotransduction currents in *dfcr* outer hair cells show weaker sensitivity and slower kinetics in response to physical displacement of hair bundles, due to the inability of *dfcr* harmonin to interact with proteins required for gating mechanotransduction channels (Grillet *et al.* 2009). These results provide an intriguing parallel to our findings that $Ca_v1.3$ properties and exocytosis are altered in *dfcr* IHCs. Other Usher syndrome-associated proteins have also been found to interact with and regulate ion channels. For example, the USH2D protein whirlin associates with $Ca_v1.3$ in photoreceptors (Kersten *et al.* 2010). The *Drosophila* homologue of whirlin, *dysc*, interacts with SLO Ca^{2+}-activated K^+ channels and enhances the expression of these channels in neurons (Jepson *et al.* 2012). Understanding how members of the Usher interactome collectively or individually alter membrane excitability and/or synaptic transmission may provide new clues into the cellular pathology leading to deafness and blindness in human patients.

References

Adato A, Michel V, Kikkawa Y, Reiners J, Alagramam KN, Weil D, Yonekawa H, Wolfrum U, El-Amraoui A & Petit C (2005). Interactions in the network of Usher syndrome type 1 proteins. *Hum Mol Genet* **14**, 347–356.

Bahloul A, Michel V, Hardelin JP, Nouaille S, Hoos S, Houdusse A, England P & Petit C (2010). Cadherin-23, myosin VIIa and harmonin, encoded by Usher syndrome type I genes, form a ternary complex and interact with membrane phospholipids. *Hum Mol Genet* **19**, 3557–3565.

Baig SM, Koschak A, Lieb A, Gebhart M, Dafinger C, Nurnberg G, Ali A, Ahmad I, Sinnegger-Brauns MJ, Brandt N, Engel J, Mangoni ME, Farooq M, Khan HU, Nurnberg P, Striessnig J & Bolz HJ (2011). Loss of Cav1.3 (*CACNA1D*) function in a human channelopathy with bradycardia and congenital deafness. *Nat Neurosci* **14**, 77–84.

Brandt A, Khimich D & Moser T (2005). Few $Ca_V1.3$ channels regulate the exocytosis of a synaptic vesicle at the hair cell ribbon synapse. *J Neurosci* **25**, 11577–11585.

Brandt A, Striessnig J & Moser T (2003). $Ca_V1.3$ channels are essential for development and presynaptic activity of cochlear inner hair cells. *J Neurosci* **23**, 10832–10840.

Calin-Jageman I & Lee A (2008). Ca_v1 L-type Ca^{2+} channel signaling complexes in neurons. *J Neurochem* **105**, 573–583.

Calin-Jageman I, Yu K, Hall RA, Mei L & Lee A (2007). Erbin enhances voltage-dependent facilitation of $Ca_v1.3$ Ca^{2+} channels through relief of an autoinhibitory domain in the $Ca_v1.3$ α_1 subunit. *J Neurosci* **27**, 1374–1385.

Chan CS, Guzman JN, Ilijic E, Mercer JN, Rick C, Tkatch T, Meredith GE & Surmeier DJ (2007). 'Rejuvenation' protects neurons in mouse models of Parkinson's disease. *Nature* **447**, 1081–1086.

Cho S, Li GL & von Gersdorff H (2011). Recovery from short-term depression and facilitation is ultrafast and Ca^{2+} dependent at auditory hair cell synapses. *J Neurosci* **31**, 5682–5692.

Cho S & von Gersdorff H (2012). Ca^{2+} influx and neurotransmitter release at ribbon synapses. *Cell Calcium* **52**, 208–216.

Christel C & Lee A (2012). Ca^{2+}-dependent modulation of voltage-gated Ca^{2+} channels. *Biochim Biophys Acta* **1820**, 1243–1252.

Christel CJ, Cardona N, Mesirca P, Herrmann S, Hofmann F, Striessnig J, Ludwig A, Mangoni ME & Lee A (2012). Distinct localization and modulation of $Ca_v1.2$ and $Ca_v1.3$ L-type Ca^{2+} channels in mouse sinoatrial node. *J Physiol* **590**, 6327–6341.

Dolphin AC (1996). Facilitation of Ca^{2+} current in excitable cells. *Trends Neurosci* **19**, 35–43.

Dou H, Vazquez AE, Namkung Y, Chu H, Cardell EL, Nie L, Parson S, Shin HS & Yamoah EN (2004). Null mutation of α_{1D} Ca^{2+} channel gene results in deafness but no vestibular defect in mice. *J Assoc Res Otolaryngol* **5**, 215–226.

Frank T, Khimich D, Neef A & Moser T (2009). Mechanisms contributing to synaptic Ca^{2+} signals and their heterogeneity in hair cells. *Proc Natl Acad Sci U S A* **106**, 4483–4488.

Goutman JD (2012). Transmitter release from cochlear hair cells is phase locked to cyclic stimuli of different intensities and frequencies. *J Neurosci* **21**, 17025–17036.

Goutman JD & Glowatzki E (2007). Time course and calcium dependence of transmitter release at a single ribbon synapse. *Proc Natl Acad Sci U S A* **104**, 16341–16346.

Goutman JD & Glowatzki E (2011). Short-term facilitation modulates size and timing of the synaptic response at the inner hair cell ribbon synapse. *J Neurosci* **31**, 7974–7981.

Graydon CW, Cho S, Li GL, Kachar B & von Gersdorff H (2011). Sharp Ca^{2+} nanodomains beneath the ribbon promote highly synchronous multivesicular release at hair cell synapses. *J Neurosci* **31**, 16637–16650.

Gregory FD, Bryan KE, Pangršič T, Calin-Jageman IE, Moser T & Lee A (2011). Harmonin inhibits presynaptic $Ca_v1.3$ Ca^{2+} channels in mouse inner hair cells. *Nat Neurosci* **14**, 1109–1111.

Grillet N, Xiong W, Reynolds A, Kazmierczak P, Sato T, Lillo C, Dumont RA, Hintermann E, Sczaniecka A, Schwander M, Williams D, Kachar B, Gillespie PG & Müller U (2009). Harmonin mutations cause mechanotransduction defects in cochlear hair cells. *Neuron* **62**, 375–387.

Hetzenauer A, Sinnegger-Brauns MJ, Striessnig J & Singewald N (2006). Brain activation pattern induced by stimulation of L-type Ca^{2+}-channels: contribution of $Ca_V1.3$ and $Ca_V1.2$ isoforms. *Neuroscience* **139**, 1005–1015.

Jenkins MA, Christel CJ, Jiao Y, Abiria S, Kim KY, Usachev YM, Obermair GJ, Colbran RJ & Lee A (2010). Ca^{2+}-dependent facilitation of $Ca_v1.3$ Ca^{2+} channels by densin and Ca^{2+}/calmodulin-dependent protein kinase II. *J Neurosci* **30**, 5125–5135.

Jepson JE, Shahidullah M, Lamaze A, Peterson D, Pan H & Koh K (2012). *dyschronic*, a *Drosophila* homolog of a deaf-blindness gene, regulates circadian output and Slowpoke channels. *PLoS Genet* **8**, e1002671.

Johnson KR, Gagnon LH, Webb LS, Peters LL, Hawes NL, Chang B & Zheng QY (2003). Mouse models of USH1C and DFNB18: phenotypic and molecular analyses of two new spontaneous mutations of the *Ush1c* gene. *Hum Mol Genet* **12**, 3075–3086.

Kersten FF, van Wijk E, van Reeuwijk J, van der Zwaag B, Marker T, Peters TA, Katsanis N, Wolfrum U, Keunen JE, Roepman R & Kremer H (2010). Association of whirlin with $Ca_v1.3$ (α_{1D}) channels in photoreceptors, defining a novel member of the usher protein network. *Invest Ophthalmol Vis Sci* **51**, 2338–2346.

Khimich D, Nouvian R, Pujol R, Tom Dieck S, Egner A, Gundelfinger ED & Moser T (2005). Hair cell synaptic ribbons are essential for synchronous auditory signalling. *Nature* **434**, 889–894.

Kimberling WJ & Moller C (1995). Clinical and molecular genetics of Usher syndrome. *J Am Acad Audiol* **6**, 63–72.

Koch M & Holt M (2012). Coupling exo- and endocytosis: an essential role for PIP_2 at the synapse. *Biochim Biophys Acta* **1821**, 1114–1132.

Koschak A, Reimer D, Huber I, Grabner M, Glossmann H, Engel J & Striessnig J (2001). α1D (Cav1.3) subunits can form L-type Ca^{2+} channels activating at negative voltages. *J Biol Chem* **276**, 22100–22106.

Lewis RS & Hudspeth AJ (1983). Voltage- and ion-dependent conductances in solitary vertebrate hair cells. *Nature* **304**, 538–541.

Li GL, Keem E, Andor-Ardo D, Hudspeth AJ & von Gersdorff H (2009). The unitary event underlying multiquantal EPSCs at a hair cell's ribbon synapse. *J Neurosci* **29**, 7558–7568.

Mangoni ME, Couette B, Bourinet E, Platzer J, Reimer D, Striessnig J & Nargeot J (2003). Functional role of L-type $Ca_v1.3$ Ca^{2+} channels in cardiac pacemaker activity. *Proc Natl Acad Sci U S A* **100**, 5543–5548.

Michalski N, Michel V, Caberlotto E, Lefèvre GM, van Aken AF, Tinevez JY, Bizard E, Houbron C, Weil D, Hardelin JP, Richardson GP, Kros CJ, Martin P & Petit C (2009). Harmonin-b, an actin-binding scaffold protein, is involved in the adaptation of mechanoelectrical transduction by sensory hair cells. *Pflugers Arch* **459**, 115–130.

Michna M, Knirsch M, Hoda JC, Muenkner S, Langer P, Platzer J, Striessnig J & Engel J (2003). $Ca_v1.3$ (α1D) Ca^{2+} currents in neonatal outer hair cells of mice. *J Physiol* **553**, 747–758.

Moser T & Beutner D (2000). Kinetics of exocytosis and endocytosis at the cochlear inner hair cell afferent synapse of the mouse. *Proc Natl Acad Sci U S A* **97**, 883–888.

Moser T, Brandt A & Lysakowski A (2006). Hair cell ribbon synapses. *Cell Tissue Res* **326**, 347–359.

Navedo MF, Amberg GC, Westenbroek RE, Sinnegger-Brauns MJ, Catterall WA, Striessnig J & Santana LF (2007). $Ca_v1.3$ channels produce persistent calcium sparklets, but $Ca_v1.2$ channels are responsible for sparklets in mouse arterial smooth muscle. *Am J Physiol Heart Circ Physiol* **293**, H1359–H1370.

Neef A, Heinemann C & Moser T (2007). Measurements of membrane patch capacitance using a software-based lock-in system. *Pflugers Arch* **454**, 335–344.

Neef J, Gehrt A, Bulankina AV, Meyer AC, Riedel D, Gregg RG, Strenzke N & Moser T (2009). The Ca^{2+} channel subunit β2 regulates Ca^{2+} channel abundance and function in inner hair cells and is required for hearing. *J Neurosci* **29**, 10730–10740.

Olson PA, Tkatch T, Hernandez-Lopez S, Ulrich S, Ilijic E, Mugnaini E, Zhang H, Bezprozvanny I & Surmeier DJ (2005). G-protein-coupled receptor modulation of striatal $Ca_V1.3$ L-type Ca^{2+} channels is dependent on a Shank-binding domain. *J Neurosci* **25**, 1050–1062.

Petit C (2001). Usher syndrome: from genetics to pathogenesis. *Annu Rev Genomics Hum Genet* **2**, 271–297.

Platzer J, Engel J, Schrott-Fischer A, Stephan K, Bova S, Chen H, Zheng H & Striessnig J (2000). Congenital deafness and sinoatrial node dysfunction in mice lacking class D L-type Ca^{2+} channels. *Cell* **102**, 89–97.

Reiners J, van Wijk E, Marker T, Zimmermann U, Jurgens K, Te Brinke H, Overlack N, Roepman R, Knipper M, Kremer H & Wolfrum U (2005). The scaffold protein harmonin (USH1C) provides molecular links between Usher syndrome type 1 and type 2. *Hum Mol Genet* **14**, 3933–3943.

Robertson D & Paki B (2002). Role of L-type Ca^{2+} channels in transmitter release from mammalian inner hair cells. II. Single-neuron activity. *J Neurophysiol* **87**, 2734–2740.

Rodriguez L, Simeonato E, Scimemi P, Anselmi F, Cali B, Crispino G, Ciubotaru CD, Bortolozzi M, Ramirez FG, Majumder P, Arslan E, De Camilli P, Pozzan T & Mammano F (2012). Reduced phosphatidylinositol 4,5-bisphosphate synthesis impairs inner ear Ca^{2+} signaling and high-frequency hearing acquisition. *Proc Natl Acad Sci U S A* **109**, 14013–14018.

Safa P, Boulter J & Hales TG (2001). Functional properties of $Ca_V1.3$ (α_{1D}) L-type Ca^{2+} channel splice variants expressed by rat brain and neuroendocrine GH_3 cells. *J Biol Chem* **276**, 38727–38737.

Sakaba T & Neher E (2001). Calmodulin mediates rapid recruitment of fast-releasing synaptic vesicles at a calyx-type synapse. *Neuron* **32**, 1119–1131.

Songyang Z, Fanning AS, Fu C, Xu J, Marfatia SM, Chishti AH, Crompton A, Chan AC, Anderson JM & Cantley LC (1997). Recognition of unique carboxyl-terminal motifs by distinct PDZ domains. *Science* **275**, 73–77.

Sueta T, Zhang SY, Sellick PM, Patuzzi R & Robertson D (2004). Effects of a calcium channel blocker on spontaneous neural noise and gross action potential waveforms in the guinea pig cochlea. *Hear Res* **188**, 117–125.

Verpy E, Leibovici M, Zwaenepoel I, Liu XZ, Gal A, Salem N, Mansour A, Blanchard S, Kobayashi I, Keats BJ, Slim R & Petit C (2000). A defect in harmonin, a PDZ domain-containing protein expressed in the inner ear sensory hair cells, underlies Usher syndrome type 1C. *Nat Genet* **26**, 51–55.

Wang CL (1985). A note on Ca^{2+} binding to calmodulin. *Biochem Biophys Res Commun* **130**, 426–430.

Wu LG & Borst JG (1999). The reduced release probability of releasable vesicles during recovery from short-term synaptic depression. *Neuron* **23**, 821–832.

Xu W & Lipscombe D (2001). Neuronal $Ca_v1.3\alpha_1$ L-type channels activate at relatively hyperpolarized membrane potentials and are incompletely inhibited by dihydropyridines. *J Neurosci* **21**, 5944–5951.

Zhang H, Fu Y, Altier C, Platzer J, Surmeier DJ & Bezprozvanny I (2006). CaV1.2 and CaV1.3 neuronal L-type calcium channels: differential targeting and signaling to pCREB. *Eur J Neurosci* **23**, 2297–2310.

Zhang H, Maximov A, Fu Y, Xu F, Tang TS, Tkatch T, Surmeier DJ & Bezprozvanny I (2005). Association of CaV1.3 L-type calcium channels with Shank. *J Neurosci* **25**, 1037–1049.

Additional information

Competing interests

None.

Author contributions

The experiments in this study were performed at the University of Iowa, Dominican University and University of Göttingen. Author contributions are as follows: conception and design of experiments, collection analysis, and interpretation of data: F.D.G., I.E.C.-J., T.P., T.M., A.L.; drafting of the article or revising it critically for important intellectual content: F.D.G., T.M., A.L. All authors approved the final version of the manuscript.

Funding

This work was supported by the NIH (DC009433, HL087120 and DC010362 to A.L.; DA015040 and K12/GM00068 to F.D.G.; and DC008417 to I.E.C.-J.), the Carver Research Program of Excellence (to A.L.), a fellowship of the Alexander von Humboldt foundation to T.P., and the German Research Foundation through the Collaborative Research Center 889 (to T.M.).